Detecting Common Signals in Multiple Time Series Using The Spectral Envelope

David S. STOFFER

One often collects p individual time series $Y_j(t)$ for $j = 1, \ldots, p$, where the interest is to discover whether any—and which—of the series contain common signals. Let $\mathbf{Y}(t) = (Y_1(t), \ldots, Y_p(t))'$ denote the corresponding $p \times 1$ vector-valued time series with $p \times p$ positive definite spectral matrix $\mathbf{f_Y}(\omega)$. Models are proposed to answer the primary question of which, if any, series have common spectral power at approximately the same frequency. These models yield a type of complex factor analytic representation for $\mathbf{f_Y}(\omega)$. A scaling approach to the problem is taken by considering possibly complex linear combinations of the components of $\mathbf{Y}(t)$. The solution leads to an eigenvalue–eigenvector problem that is analogous to the spectral envelope and optimal scaling methodology first presented by Stoffer, Tyler, and McDougall. The viability of the techniques is demonstrated by analyzing data from an experiment that assessed pain perception in humans and by analyzing data from a study of ambulatory blood pressure in a cohort of preteens.

KEY WORDS: Ambulatory blood pressure; Factor analysis; Fourier analysis; Functional magnetic resonance imaging; Latent roots and vectors; Optimal scaling; Principal components; Random frequency effects; Signal detection; Spectral envelope.

1. INTRODUCTION

Frequently, $p > 1$ time series $\{Y_j(t), t = 1, \ldots, n_j\}$ for $j = 1, \ldots, p$, are collected with the primary interest being whether any—and how many—have common cyclic components. The series need not be in phase, and the sample lengths, n_j, need not be the same, but must be of the same magnitude. In this case a common sample length, n, that is highly composite is chosen, and the data are padded or shortened accordingly. The problem of whether *all* of the series contain unspecified fundamental harmonics was discussed by MacNeill (1977). The method can be viewed as an extension of Fisher's method for discovering a periodic component and suffers from the same problems. Basically, the technique tests whether all of the series have the same r fundamental harmonics by looking at the $(m - r)$th order statistic of $D_l = \min\{I_{11}(2\pi l/n), \ldots, I_{pp}(2\pi l/n)\}, l = 1, \ldots, m = [(n - 1)/2]$, where $I_{jj}(\cdot)$ is a normalized periodogram of the jth series. Another approach to this problem is spectral domain factor analysis (see, e.g. Geweke 1977). Some drawbacks of the factor analytic method are that as it has been developed, it requires the unknown signal to be generated by a linear process and that all series be in phase. This is also true for Brillinger's (1980) spectral domain analysis of variance approach.

This approach grew out of the need to analyze multiple time series without having to make restrictive assumptions about the nature of the signal, and with the knowledge that the signals may be only approximately the same. It may also be the case that some of the series being analyzed do not have any signal. For example, in humans, body temperature, hormone levels, heart rate, and blood pressure typically follow circadian rhythms. These rhythms are approximate and, for example, if we were to make ambulatory blood pressure readings on many subjects, then we would expect the signal frequency to vary slightly from subject to subject, but for all intents and purposes, these rhythms would be considered the same. In addition, we would not expect all of the subjects' blood pressures to be rhythmic. An example examining the diastolic blood pressure of preteens is considered in Section 4. Another example of the kind of data that one can analyze is as follows.

Example 1: An Experiment in Pain Using Functional Magnetic Resonance Imaging. In this experiment functional magnetic resonance imaging (fMRI) was used to examine pain perception in humans. Two types of stimuli were presented to awake subjects: electric shock (15 mA, 2 Hz) and a nonpainful brush on the subject's hand. The effects of general anesthesia on pain perception were evaluated by comparing results from alert volunteers with those from the same volunteers while anesthetized and paralyzed with .15 mg/kg vecuronium. Data were also collected under two anesthetic conditions, .7% (low) and 1.3% (high) isoflurane. During the anesthetized conditions, a supramaximal shock (50 mA, 100 Hz) stimulus was added. This stimulus was used to simulate surgical incision without inflicting tissue damage. The stimulus conditions were [1] awake-brush (five subjects), [2] awake-shock (five subjects), [3] low-brush (three subjects), [4] low-supramaximal shock (four subjects), [5] high-brush (four subjects), and [6] high-supramaximal shock (five subjects). The specific locations of the brain where the signal was measured were [L1] cortex: primary somatosensory, contralateral; [L2] cortex: primary somatosensory, ipsilateral; [L3] cortex: secondary somatosensory, contralateal; [L4] cortex: secondary somatosensory, ipsilateral; [L5] caudate; [L6] thalamus: contralateral; [L7] thalamus: ipsilateral; [L8] cerebellum: contralateral; and [L9] cerebellum: ipsilateral.

The data comprise consecutive measures of blood oxygenation level dependent (BOLD) signal intensity (for details, see Ogawa and Lee 1990 and Ogawa, Lee, Nayak, and Glynn 1990). Areas of activation were analyzed over time at the level of the voxel, or three-dimensional pixel;

David S. Stoffer is Professor, Department of Statistics, University of Pittsburgh, PA 15260 (E-mail: *stoffer@stat.pitt.edu*). This work was supported, in part, by a grant from the National Science Foundation.

the voxel with the highest activation was chosen from each brain location. The sampling rate was one observation every 2 seconds for 256 seconds ($n = 128$). Each stimulus was applied for 32 seconds and then stopped for 32 seconds; thus the signal period is 64 seconds, and the signal is nonsinusoidal. For this analysis, I averaged over subjects in each stimulus condition (these were evoked responses and all subjects were in phase) producing data, $Y_j(t)$, for each stimulus condition [1]–[6]. Thus for a given stimulus condition, $Y_j(t)$ represents the average BOLD signal intensity at location j, for $j = 1, \ldots, 9$, at time point t, for $t = 1, \ldots, 128$.

The types of data encountered in this experiment are quite varied. For example, Figure 1 shows the nine time series, one for each location, of the stimulus condition awake-shock. It is clear from the data that in this case many locations received the shock signal of approximately four cycles in 128 points. Figure 2 shows the nine series for the stimulus condition high-brush, which is quite different than Figure 1, and it is not clear whether or not any location received any signal, or if signals are being received, whether or not they are being received in phase (at the same time). The main interest is in which locations are receiving the stimulus signal. A secondary question focuses on whether or not the locations are receiving the signals in phase. These questions are discussed further in Section 4.

In this article the concept of the *spectral envelope,* first presented by Stoffer, Tyler, and McDougall (1993) for categorical time series and by McDougall, Stoffer, and Tyler (1997) for real-valued time series, is extended to analyzing multiple time series collected in a simple experimental design. First, we develop a general approach to handle the case where data can contain the same harmonic components, and then we present the more difficult problem of analyzing approximate signals as previously mentioned.

As a general description, the spectral envelope is a frequency-based principal components technique applied to multivariate time series. Most of the technical details have been given by Stoffer, Tyler, and McDougall (1993); this technique is also related to Brillinger's (1975, chap. 9) principal components methods. Briefly, if $\mathbf{Y}(t)$ is a $p \times 1$ vector-valued time series with $p \times p$ nonsingular spectral density matrix $\mathbf{f_Y}(\omega)$, then we define the univariate process $X(t;\boldsymbol{\beta})$ by $X(t;\boldsymbol{\beta}) = \boldsymbol{\beta}^*\mathbf{Y}(t)$, where $\boldsymbol{\beta}$ is a $p \times 1$ vector of constants (that are not all 0), which may be real or complex. The * means to transpose and conjugate. We call $X(t;\boldsymbol{\beta})$ the *scaled* process, because it is obtained by scaling the vector process $\mathbf{Y}(t)$. The goal is to find such vectors so that the standardized spectral density of $X(t;\boldsymbol{\beta})$, say $f_X(\omega,\boldsymbol{\beta})/\sigma^2_{\boldsymbol{\beta}}$, where $\sigma^2_{\boldsymbol{\beta}} = \mathrm{var}\{X(t;\boldsymbol{\beta})\}$, is in some sense interesting. In this particular setting, for each frequency, $\boldsymbol{\beta}(\omega)$ is called the *optimal scaling* at frequency ω if it satisfies

$$\lambda(\omega) = \sup_{\boldsymbol{\beta}\neq\mathbf{0}} \left\{ \frac{f_X(\omega;\boldsymbol{\beta})}{\sigma^2_{\boldsymbol{\beta}}} \right\}. \tag{1}$$

Note that $\lambda(\omega)$ can be thought of as the largest proportion of the power (variance) that can be obtained at frequency ω for any scaling of the time series $\mathbf{Y}(t)$, and $\boldsymbol{\beta}(\omega)$ is the particular scaling that maximizes the power at frequency ω. Thus $\lambda(\omega)$ is called the spectral envelope. The term "spectral envelope" is appropriate because $\lambda(\omega)$ envelopes the spectrum of any scaled process. That is, for any linear combination of the elements of $\mathbf{Y}(t)$, the standardized spectral density of the resulting univariate series is no bigger than the spectral envelope, with equality only when the scale vector, $\boldsymbol{\beta}$, is proportional to the optimal scaling, $\boldsymbol{\beta}(\omega)$.

Because $X(t,\boldsymbol{\beta}) = \boldsymbol{\beta}^*\mathbf{Y}(t)$, this relationship implies that

$$\lambda(\omega) = \sup_{\boldsymbol{\beta}\neq\mathbf{0}} \left\{ \frac{\boldsymbol{\beta}^*\mathbf{f_Y}(\omega)\boldsymbol{\beta}}{\boldsymbol{\beta}^*\mathbf{V_Y}\boldsymbol{\beta}} \right\}, \tag{2}$$

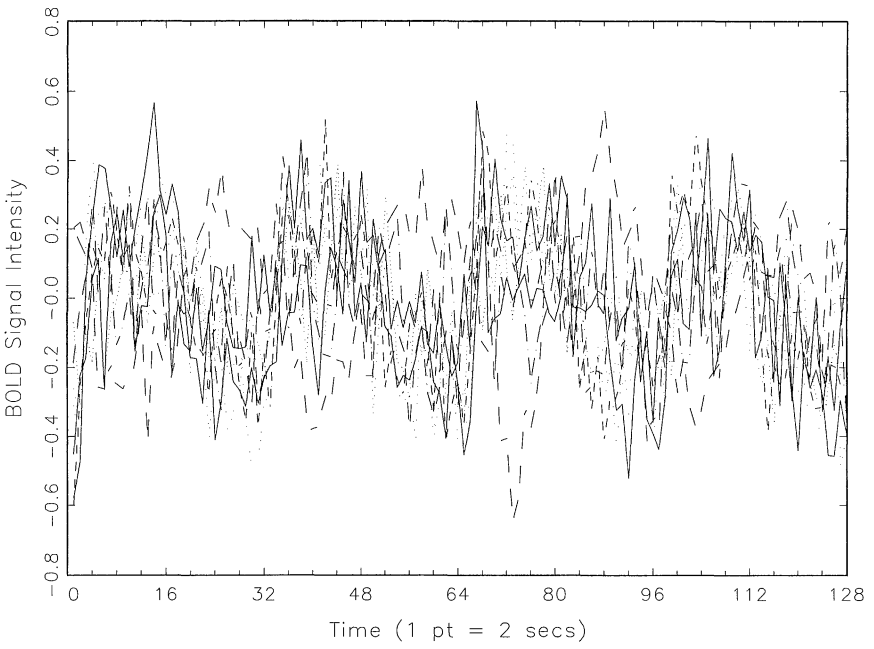

Figure 1. The BOLD Signal Intensities at all Nine Locations for the Stimulus Condition Awake-Shock.

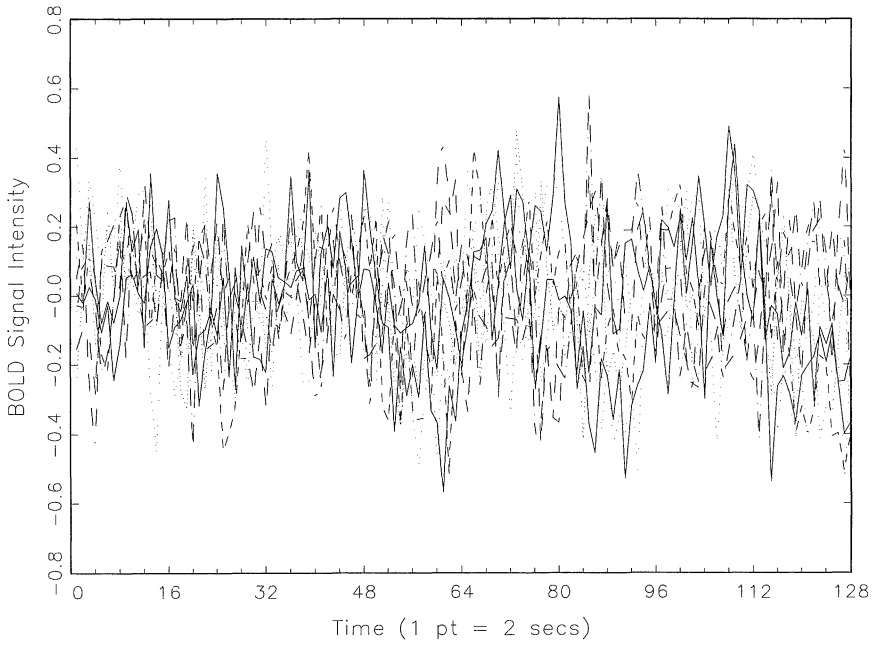

Figure 2. The BOLD Signal Intensities at all Nine Locations for the Stimulus Condition High-Brush.

where $\mathbf{V_Y}$ is the positive definite variance–covariance matrix of $\mathbf{Y}(t)$. It follows from (2) that $\lambda(\omega)$ is the (real-valued) largest eigenvalue associated with the determinantal equation

$$|\mathbf{f_Y}(\omega) - \lambda \mathbf{V_Y}| = 0, \tag{3}$$

and $\boldsymbol{\beta}(\omega)$ is the corresponding eigenvector satisfying

$$\mathbf{f_Y}(\omega)\boldsymbol{\beta}(\omega) = \lambda(\omega)\mathbf{V_Y}\boldsymbol{\beta}(\omega), \tag{4}$$

subject to constraint $\boldsymbol{\beta}(\omega)^* \mathbf{V_Y} \boldsymbol{\beta}(\omega) = 1$.

If we restrict attention to real-valued scales [i.e., $X(t;\boldsymbol{\beta}) = \boldsymbol{\beta}'\mathbf{Y}(t)$, where $\boldsymbol{\beta}$ is real-valued], then although $\mathbf{f_Y}(\omega)$ is complex, the following relationship holds: $\boldsymbol{\beta}'\mathbf{f_Y}(\omega)\boldsymbol{\beta} = \boldsymbol{\beta}'\mathbf{f}_\mathbf{Y}^{\mathrm{re}}(\omega)\boldsymbol{\beta}$, where $\mathbf{f}_\mathbf{Y}^{\mathrm{re}}(\omega)$ denotes the real part of $\mathbf{f_Y}(\omega)$. It follows that $\lambda(\omega)$ and $\boldsymbol{\beta}(\omega)$ can be easily obtained by solving an eigenvalue problem with real-valued positive definite matrices. That is, $\lambda(\omega)$ is the largest eigenvalue of $\mathbf{f}_\mathbf{Y}^{\mathrm{re}}(\omega)$ in the metric of $\mathbf{V_Y}$, and $\boldsymbol{\beta}(\omega)$ is the corresponding eigenvector.

The viability of the spectral envelope for solving the stated signal detection problems comes from the following simple observation. If the $Y_j(t)$ are of the "signal plus independent noise" form, say $Y_j(t) = S(t) + \varepsilon_j(t)$, then in terms of spectra, $f_{Y_j}(\omega) = f_S(\omega) + \sigma_\varepsilon^2$, using obvious notation, where $\mathrm{var}(\varepsilon_j) = \sigma_\varepsilon^2$ for $j = 1, \ldots, p$. The average of the $Y_j(t)$, say $X(t; p^{-1}\mathbf{1}) = p^{-1}\mathbf{1}'\mathbf{Y}(t)$, where $\mathbf{Y}(t) = (Y_1(t), \ldots, Y_p(t))'$ and $\mathbf{1}$ is a vector of 1's, will have spectrum $f_X(\omega; p^{-1}\mathbf{1}) = f_S(\omega) + p^{-1}\sigma_\varepsilon^2$. Thus the signal-to-noise ratio of $X(t, p^{-1}\mathbf{1})$ has increased by a factor of p over the individual series.

2. A MODEL AND AN EXAMPLE

In this section I suppose that the data $Y_j(t)$ can be written as the sum of K independent random signals; that is,

$$Y_j(t) = \mu_j + \sum_{k=1}^{K} c_{kj} S_k(t - \tau_{kj}) + \varepsilon_j(t), \qquad j = 1, \ldots, p \tag{5}$$

where μ_j is the mean level of the jth series; $S_k(t)$ are independent, zero mean, unit variance random signals with spectra $f_{S_k}(\omega)$; c_{kj} are the signal amplitudes (any of which may be 0) corresponding to the jth series; and the $\varepsilon_j(t)$ are independent white noise processes with variance σ_j^2 and independent of the $S_k(t)$. The individual phases, τ_{kj}, need not be integral, and it may be the case that all series are in phase; that is, $\tau_{k1} = \cdots = \tau_{kp} = 0$ for $k = 1, \ldots, K$ (e.g., evoked responses).

Denote the discrete Fourier transforms (DFTs) of the $Y_j(t)$ by $d_{Y_j}(\omega)$ for $j = 1, \ldots, p$; that is,

$$d_{Y_j}(\omega) = n^{-1/2} \sum_{t=1}^{n} Y_j(t) \exp(-2\pi i t \omega). \tag{6}$$

They are evaluated over ω in the set of positive fundamental frequencies $\{\omega = l/n; l = 1, 2, \ldots, [(n-1)/2]\}$. In terms of the model (5), these can be written as

$$d_{Y_j}(\omega) = \sum_{k=1}^{K} a_{kj} d_{S_k}(\omega) + d_{\varepsilon_j}(\omega), \tag{7}$$

where $d_{S_k}(\omega), k = 1, \ldots, K, d_{\varepsilon_j}(\omega)$ represent the DFTs of the signals and of the noise, and $a_{kj} = c_{kj} \exp(-2\pi i \tau_{kj} \omega)$.

Let $\mathbf{Y}(t) = (Y_1(t), \ldots, Y_p(t))'$ be the vector of observations, and let $\mathbf{d_Y}(\omega)$ denote the $p \times 1$ vector of transforms with jth component $d_{Y_j}(\omega)$. Then (7) can be written as

$$\mathbf{d_Y}(\omega) = \sum_{k=1}^{K} \mathbf{a}_k d_{S_k}(\omega) + \mathbf{d}_\varepsilon(\omega), \tag{8}$$

where $\mathbf{a}_k$ is the $p \times 1$ complex vector $\mathbf{a}_k = (a_{k1}, \ldots, a_{kp})'$ and $\mathbf{d}_\varepsilon(\omega)$ is the $p \times 1$ vector of transforms with jth component $d_{\varepsilon_j}(\omega)$.

From (8), a variance components model for the transforms can be identified in terms of the respective spectra; that is,

$$\mathbf{f}_\mathbf{Y}(\omega) = \sum_{k=1}^{K} \mathbf{a}_k f_{S_k}(\omega)\mathbf{a}_k^* + \mathbf{f}_\varepsilon(\omega), \tag{9}$$

where $\mathbf{f}_\mathbf{Y}(\omega)$ is the $p \times p$ positive definite Hermitian spectral matrix of the observation vector $\mathbf{Y}(t)$, $f_{S_k}(\omega)$ is the scalar real-valued spectrum of the signal $S_k(t)$ for $k = 1, \ldots, K$, and $\mathbf{f}_\varepsilon(\omega)$ is the $p \times p$ diagonal, real, positive definite matrix given by $\mathbf{f}_\varepsilon(\omega) \equiv \operatorname{diag}\{\sigma_1^2, \ldots, \sigma_p^2\}$. Note that $\mathbf{f}_\varepsilon(\omega)$ is constant with respect to frequency.

The assumption on the signals $S_k(t)$, and hence on their spectra $f_{S_k}(\omega)$, for $k = 1, \ldots, K$, is that they are narrow band and that the peaks are well separated. Thus from a practical standpoint, at any particular frequency ω, the model (9) reduces to a single-signal model (i.e., $K = 1$). As described in Section 1, the spectral envelope, $\lambda(\omega)$, is a frequency-dependent investigation in that its optimality criterion focuses on individual frequencies. That is, if $\lambda(\omega_0)$ is the spectral envelope at frequency ω_0, then the corresponding optimal scaling, $\boldsymbol{\beta}(\omega_0)$, is optimal at ω_0 but not necessarily anywhere else. Hence I focus on the case where $K = 1$ and drop k from the notation.

The model I work with is given by

$$\mathbf{f}_\mathbf{Y}(\omega) = \mathbf{a} f_S(\omega)\mathbf{a}^* + \mathbf{f}_\varepsilon(\omega), \tag{10}$$

where the scalar signal spectrum is written as $f_S(\omega)$. The vector $\mathbf{a}$ is now a $p \times 1$ complex vector, with elements of the form $a_j = c_j \exp(-2\pi i \tau_j \omega)$, for $j = 1, \ldots, p$. If component j does not contain the signal, then $c_j = 0$ (and hence $a_j = 0$), and (10) is arranged so that for $0 \le q \le p, a_{q+1} = \cdots = a_p = 0$, and none of the $\{a_1, \ldots, a_q\}$ are 0. Thus in (10), $\mathbf{a} f_S(\omega)\mathbf{a}^*$ is a Hermitian block-diagonal matrix with 0's everywhere except the upper $q \times q$ block, and $\mathbf{f}_\varepsilon(\omega) = \operatorname{diag}\{\sigma_1^2, \ldots, \sigma_p^2\}$ is a real diagonal matrix.

Rather than work with the original series, I prefer to work with the standardized series, $\mathbf{Z}(t) = \mathbf{V}^{-1/2}\mathbf{Y}(t)$, where $\mathbf{V} = \operatorname{diag}\{\sigma_{Y_1}^2, \ldots, \sigma_{Y_p}^2\}$ with $\sigma_{Y_j}^2 = \operatorname{var}\{Y_j(t)\}$. Note that the diagonal elements of $\mathbf{V}$ get contributions from both the signals (if any are present) and the noise; that is, $\sigma_{Y_j}^2 = \sum_{k=1}^{K} c_{kj}^2 + \sigma_j^2$, where any or all of the c_{kj} could be 0. Writing (10) in terms of the standardized processes, $\mathbf{Z}(t)$,

$$\mathbf{f}_\mathbf{Z}(\omega) = \mathbf{a}(\omega)\mathbf{a}^*(\omega) + \mathbf{D}(\omega). \tag{11}$$

Note that (11) is a type of complex factor-analytic representation for

$$\mathbf{f}_\mathbf{Z}(\omega) = \mathbf{V}^{-1/2}\mathbf{f}_\mathbf{Y}(\omega)\mathbf{V}^{-1/2}; \tag{12}$$

that is, $\mathbf{f}_\mathbf{Z}(\omega)$ is the sum of a rank 1, nonnegative definite Hermitian matrix, $\mathbf{a}(\omega)\mathbf{a}^*(\omega)$, and a diagonal positive definite matrix, $\mathbf{D}(\omega)$, where $\mathbf{a}(\omega)$ is a $p \times 1$ complex-valued vector such that

$$\mathbf{a}(\omega)\mathbf{a}^*(\omega) = \mathbf{V}^{-1/2}\mathbf{a} f_S(\omega)\mathbf{a}^*\mathbf{V}^{-1/2}, \tag{13}$$

and the final $p-q$ elements of $\mathbf{a}(\omega)$ are 0. The value q corresponds to the number of elements that contain the particular signal associated with frequency ω. In addition, I restrict attention to case where

$$\mathbf{D}(\omega) = \mathbf{V}^{-1/2}\mathbf{f}_\varepsilon(\omega)\mathbf{V}^{-1/2} \tag{14}$$

is constant over ω; that is, $\mathbf{D}(\omega) \equiv \operatorname{diag}\{\sigma_1^2/\sigma_{Y_1}^2, \ldots, \sigma_p^2/\sigma_{Y_p}^2\}$. Because $f_S(\omega)$ is real, if the series are in phase with respect to this particular signal (i.e., $\tau_1 = \cdots = \tau_q = 0$), then $\mathbf{f}_\mathbf{Z}(\omega)$ will also be real.

To apply the spectral envelope to the standardized series, let $\boldsymbol{\beta} \neq \mathbf{0}$ be a complex-valued $p \times 1$ vector of scalings and consider the standardized scaled complex series, $X(t; \boldsymbol{\beta}) = \boldsymbol{\beta}^*\mathbf{Z}(t)$. One may now write

$$f_X(\omega, \boldsymbol{\beta}) = \boldsymbol{\beta}^*\mathbf{f}_\mathbf{Z}(\omega)\boldsymbol{\beta}, \tag{15}$$

where $f_X(\omega, \boldsymbol{\beta})$ is the spectral density of $X(t; \boldsymbol{\beta})$. If it is believed that the series are in phase with respect to this particular signal ($\tau_1 = \cdots = \tau_q = 0$), then there is no particular advantage to considering complex-valued scales, and one would restrict $\boldsymbol{\beta}$ to be a vector of real scalings. For generality, I focus on the complex case.

The goal is to find $\boldsymbol{\beta}$, at each ω, to maximize (15), subject to the constraint $\boldsymbol{\beta}^*\boldsymbol{\beta} = 1$. I denote the solution by $\boldsymbol{\beta}(\omega)$. Setting $\mathbf{b} = \mathbf{V}^{-1/2}\boldsymbol{\beta}$ leads to the optimality criterion

$$\lambda(\omega) = \sup_{\mathbf{b} \neq \mathbf{0}} \left\{ \frac{\mathbf{b}^*\mathbf{f}_\mathbf{Y}(\omega)\mathbf{b}}{\mathbf{b}^*\mathbf{V}\mathbf{b}} \right\}. \tag{16}$$

The function $\lambda(\omega)$ is the spectral envelope, because $f_X(\omega, \boldsymbol{\beta}) \le \lambda(\omega)$, for any scaling $\boldsymbol{\beta}$, with equality when $\boldsymbol{\beta} \propto \boldsymbol{\beta}(\omega)$. The corresponding scaling, $\boldsymbol{\beta}(\omega)$, is the optimal scaling. As mentioned in Section 1, the idea in using (16) is that the right (perhaps complex) linear combination of the p series, namely $X(t; \boldsymbol{\beta}(\omega))$, will enhance the signal and dampen the noise. Note that the role of $\boldsymbol{\beta}$ in this section is slightly different than in the previous section, because I am working with the standardized series. If $\mathbf{V} = \operatorname{diag}\{\sigma_{Y_1}^2, \ldots, \sigma_{Y_p}^2\}$ in (16) is replaced by $\mathbf{V}_\mathbf{Y} = \operatorname{var}\{\mathbf{Y}(t)\}$, then $\mathbf{b}$ in (16) is the $\boldsymbol{\beta}$ of Section 1. The reason that $\mathbf{V}$ is preferred over $\mathbf{V}_\mathbf{Y}$ in this problem is that using $\mathbf{V}$ leads to the simple decomposition of (11)–(14). In addition, simulation studies have shown that using $\mathbf{V}$ is superior to $\mathbf{V}_\mathbf{Y}$ in identifying signals.

The solution to (16) is obtained by finding, at each Fourier frequency ω, the largest eigenvalue, $\lambda(\omega)$, and corresponding eigenvector, $\boldsymbol{\beta}(\omega)$, of the matrix $\mathbf{f}_\mathbf{Z}(\omega)$ given in (12), which, as previously stated, is the sum of the block-diagonal matrix (with nonzero values only in the upper $q \times q$ portion) $\mathbf{a}(\omega)\mathbf{a}^*(\omega)$ given in (13) and the diagonal real matrix $\mathbf{D}(\omega)$ given in (14), which is constant with respect to ω. From this, it is seen that if there is a harmonic component near ω in q of the p series, then $\lambda(\omega)$ will be "large," and the final $p-q$ components of $\boldsymbol{\beta}(\omega)$ will be 0. In regions where there is no harmonic component, $f_S(\omega)$ will be negligible, so that $\lambda(\omega)$ will be flat and the final $p-q$ components of $\boldsymbol{\beta}(\omega)$ will not be 0—in fact, the modulus of those $p-q$ elements

may dominate the first q elements if the signal amplitudes are large. These facts will lead to reasonable conclusions about the nature of the signal and the number of elements q that contain the signal. I have also found that it is worthwhile to look at the unstandardized results; that is, replace $\mathbf{V}$ with the identity matrix in (16); this aids identification of interesting frequencies.

There are many methods for obtaining consistent and efficient estimators of $\mathbf{f}_\mathbf{Y}(\omega)$ (see, e.g., Brillinger 1975, chap. 7; Hannan 1970, chap. 5). One particular method is by smoothing the $p \times p$ periodogram matrices, $\mathbf{I}_n(\omega) = \mathbf{d}_\mathbf{Y}(\omega)\mathbf{d}_\mathbf{Y}^*(\omega)$. Let $\omega_l = l/n$ be the lth Fourier frequency and denote the $p \times p$ sample spectral matrix by

$$\hat{\mathbf{f}}_\mathbf{Y}(\omega_l) = \sum_{r=-m}^{m} h_r \mathbf{I}_n(\omega_{l+r}), \tag{17}$$

where $\{h_r\}$ are symmetric ($h_r = h_{-r}$) positive weights that sum to unity and m, which is a function of n, controls the degree of smoothness. For $\hat{\mathbf{f}}_\mathbf{Y}(\omega_l)$ to be consistent, the weights must satisfy $\sum h_r^2 \to 0$ for $m, n \to \infty$. I concentrate on the estimator described in (17), but in general, $\hat{\mathbf{f}}_\mathbf{Y}(\omega)$ may be any consistent and efficient estimator of the spectral matrix $\mathbf{f}_\mathbf{Y}(\omega)$.

Denoting the diagonal matrix of sample variances by $\hat{\mathbf{V}}$, the sample spectral envelope, $\hat{\lambda}(\omega_l)$, is the largest eigenvalue of

$$\hat{\mathbf{f}}_\mathbf{Z}(\omega_l) = \hat{\mathbf{V}}^{-1/2}\hat{\mathbf{f}}_\mathbf{Y}(\omega_l)\hat{\mathbf{V}}^{-1/2}, \tag{18}$$

and the sample optimal scaling, $\hat{\boldsymbol{\beta}}(\omega_l)$, is the corresponding eigenvector. The elements of $\hat{\boldsymbol{\beta}}(\omega_l)$ can be inspected to determine which of the series contain the signal.

If $\boldsymbol{\beta}$ is restricted to be real, then one retains only the real part of $\hat{\mathbf{f}}_\mathbf{Y}(\omega_l)$, say $\hat{\mathbf{f}}_\mathbf{Y}^{\mathrm{re}}(\omega)$, in the calculations performed in (17) and (18). In this case, the results of Stoffer et al. (1993, thms. 3.1–3.3) apply. As a summary, the results state that if $\lambda(\omega)$ is a distinct root (which implies that $\lambda(\omega) > 0$), then, independently for large n and m (put $m \equiv m_n$ and take $m_n \to \infty$ as $n \to \infty$ but with $m_n/n \to 0$),

$$\nu_m[\hat{\lambda}(\omega) - \lambda(\omega)]/\lambda(\omega)$$
has a standard normal distribution, (19)

and

$$\nu_m[\hat{\boldsymbol{\beta}}(\omega) - \boldsymbol{\beta}(\omega)]$$
has a multivariate normal distribution, (20)

where the term ν_m depends on the type of estimator used. In the case of (17), $\nu_m^{-2} = \sum_{r=-m}^{m} h_r^2$; if a simple average is

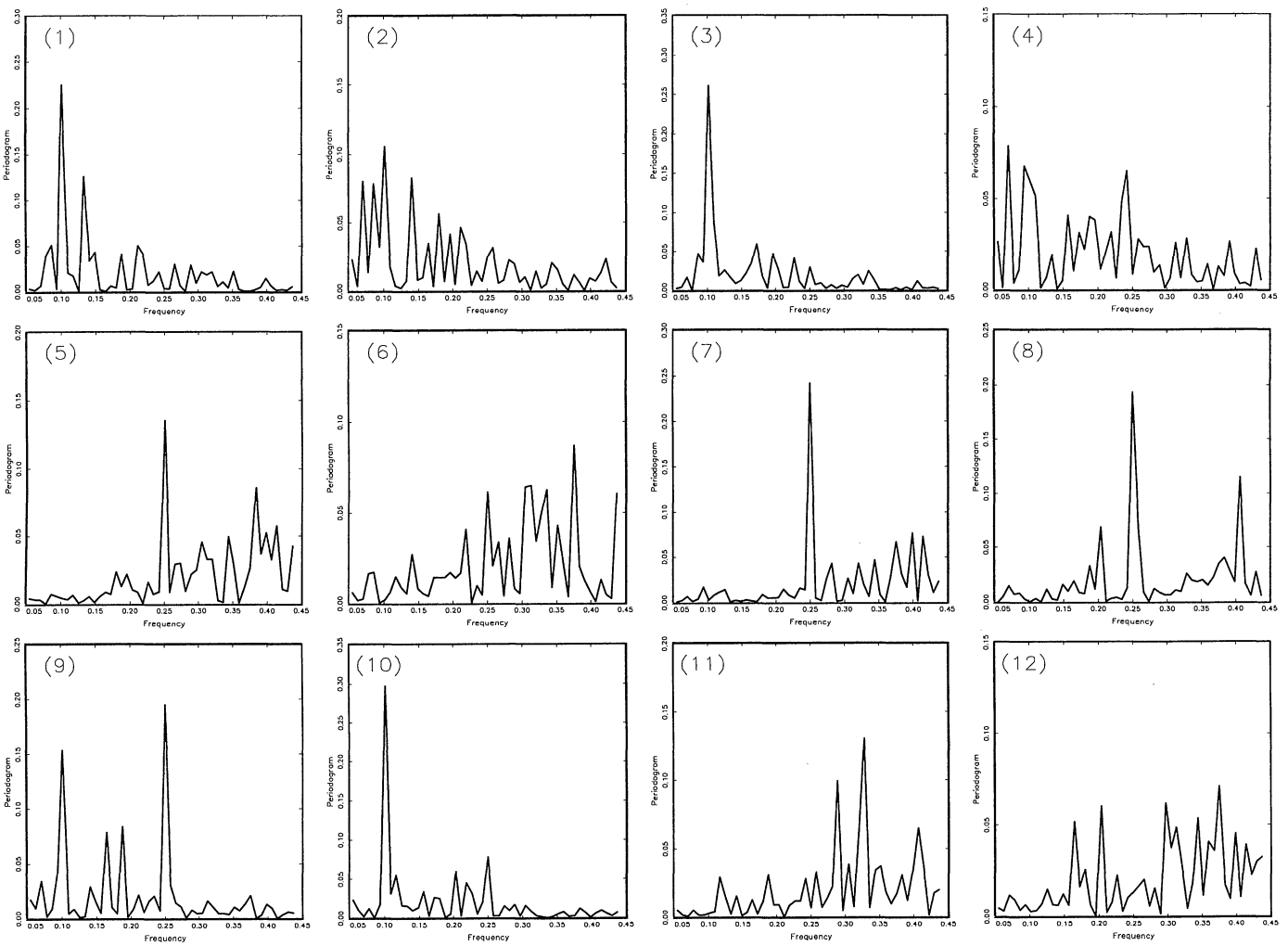

Figure 3. Periodograms of the Time Series $Y_j(t)$, for $j = 1, \ldots, 12$, Generated in Example 2.

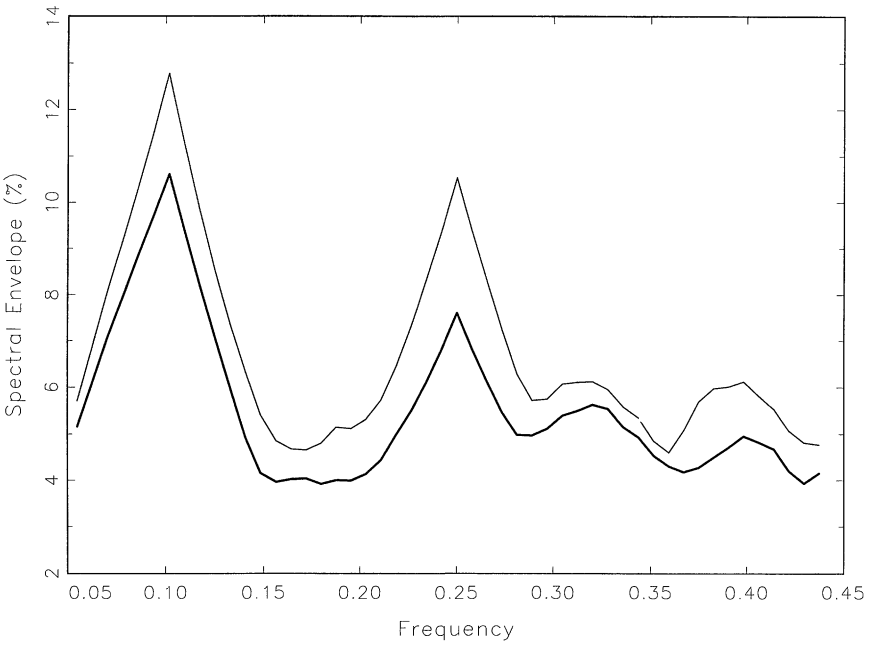

Figure 4. Spectral Envelopes of the 12 Time Series Generated in Example 2, Based on Complex Scales (Thin Line) and on Real Scales (Thick Line).

used, $h_r = 1/(2m+1)$, then $\nu_m^2 = (2m+1)$. Based on these results, asymptotic normal confidence intervals and tests for $\lambda(\omega)$ can be readily constructed. Similarly, for $\boldsymbol{\beta}(\omega)$, asymptotic confidence ellipsoids and chi-squared tests can be constructed. In particular, a simple asymptotic test statistic for $\boldsymbol{\beta}(\omega)$ can be obtained. Let $\hat{\mathbf{H}}(\omega) = \hat{\mathbf{f}}_{\mathbf{Y}}^{\mathrm{re}}(\omega) - \hat{\lambda}(\omega)\mathbf{I}_p$, where $\mathbf{I}_p$ is the $p \times p$ identity matrix, and

$$\boldsymbol{\xi}_m(\omega) = \sqrt{2}\nu_m \hat{\mathbf{f}}_{\mathbf{Y}}^{\mathrm{re}}(\omega)^{-1/2}\hat{\mathbf{H}}(\omega)(\hat{\boldsymbol{\beta}}(\omega) - \boldsymbol{\beta}(\omega))/\hat{\lambda}(\omega)^{1/2}.$$

Then

$$\boldsymbol{\xi}_m(\omega)'\boldsymbol{\xi}_m(\omega) \tag{21}$$

converges $(m, n \to \infty)$ in distribution to a distribution that is stochastically less than χ^2_{p-1} and stochastically greater than χ^2_{p-2}. Note that the test statistic (21) is 0 if $\boldsymbol{\beta}(\omega)$ is replaced by $\hat{\boldsymbol{\beta}}(\omega)$. One can check whether or not a particular element of $\hat{\boldsymbol{\beta}}(\omega)$ is 0 by inserting $\hat{\boldsymbol{\beta}}(\omega)$ for $\boldsymbol{\beta}(\omega)$, but with the particular element zeroed out and the resulting vector rescaled to be of unit length, into (21).

For practical purposes, the following method can be used to inspect the spectral envelope for peaks. Using a first-order Taylor expansion,

$$\log \hat{\lambda}(\omega) \approx \log \lambda(\omega) + \frac{\hat{\lambda}(\omega) - \lambda(\omega)}{\lambda(\omega)}, \tag{22}$$

so that in view of (19), $\nu_m[\log \hat{\lambda}(\omega) - \log \lambda(\omega)]$ is approximately standard normal. If no signal is present in a sequence of length n, then one would expect $\lambda(\omega_l) \approx 2/n$ for $1 < l < n/2$, and hence approximately $(1-\alpha)\times 100\%$ of the time, $\log \hat{\lambda}(\omega_l)$ will be less than $\log(2/n) + (z_\alpha/\nu_m)$, where z_α is the $(1-\alpha)$ upper tail cutoff of the standard normal distribution. Exponentiating, the α critical value for $\hat{\lambda}(\omega_l)$ becomes $(2/n)\exp(z_\alpha/\nu_m)$. Although this method is a bit crude, from my experience, thresholding at very small

Table 1. Example 2 Results for Frequency ω = .10

Series	Amplitude	Complex scale [a,b]	Real scale [a,c]
1	.59	.51 (179.59)	.49 (74.60)
2	.36	.29 (148.47)	.38 (40.08)
3	.87	.52 (368.31)	.55 (75.76)
4	.21	.25 (31.20)	.27 (12.53)
5	0	.05 (12.34)	.06 (4.56)
6	0	.06 (8.35)	.02 (0.56)
7	0	.04 (3.53)	.01 (0.10)
8	0	.03 (2.24)	.01 (0.39)
9	.34	.36 (107.62)	.27 (15.34)
10	.84	.43 (155.14)	.41 (22.50)
11	0	.05 (5.99)	.02 (0.40)
12	0	.03 (3.39)	.05 (2.29)

NOTE: [a]Values shown are the absolute values of the particular scale.
[b]The value of the test statistic based on (23) is shown in parentheses; compare cautiously to a χ^2_{22}.
[c]The value of the test statistic based on (21) is shown in parentheses; compare cautiously to a χ^2_{10}.

Table 2. Example 2 Results for Frequency ω = .25

Series	Amplitude	Complex scale [a,b]	Real scale [a,c]
1	0	.07 (2.49)	.04 (.34)
2	0	.18 (65.82)	.19 (10.70)
3	0	.17 (24.99)	.07 (.81)
4	0	.13 (8.89)	.19 (6.08)
5	.62	.36 (179.44)	.37 (47.21)
6	.39	.25 (101.66)	.32 (31.62)
7	1.06	.50 (172.54)	.53 (39.39)
8	.54	.40 (223.99)	.44 (55.85)
9	.37	.42 (205.44)	.35 (15.95)
10	.48	.29 (92.94)	.28 (14.55)
11	0	.12 (14.75)	.04 (.28)
12	0	.12 (12.36)	.10 (3.86)

NOTE: [a]Values shown are the absolute values of the particular scale.
[b]The value of the test statistic based on (23) is shown in parentheses; compare cautiously to a χ^2_{22}.
[c]The value of the test statistic based on (21) is shown in parentheses; compare cautiously to a χ^2_{10}.

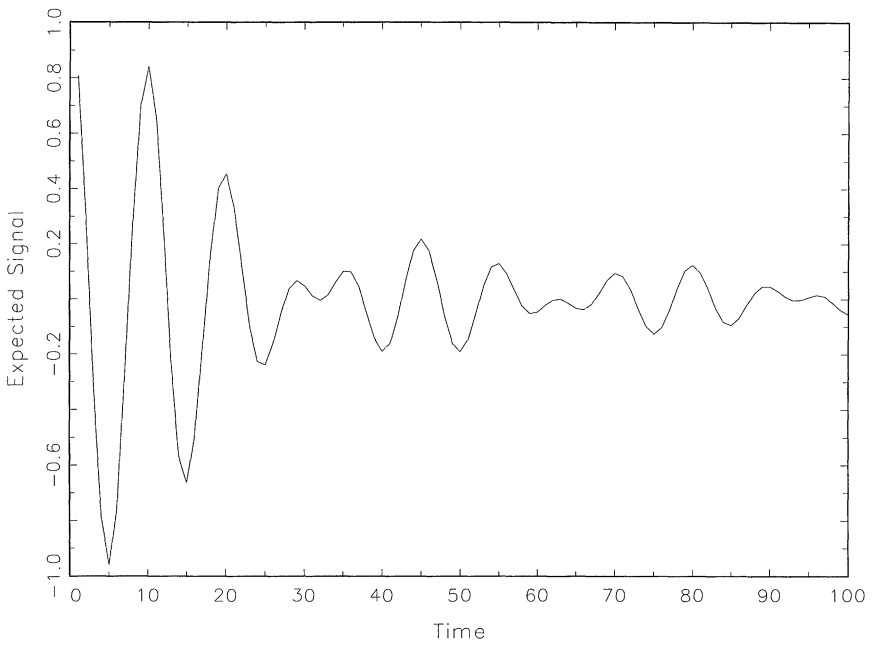

Figure 5. Expected Value of the Signal as Given by (27) With ω_0 = .1 and Δ = .1/(2π) = .016.

α levels (say, $\alpha = 10^{-3}$ to 10^{-6}, depending on the size on n) works well.

If $\boldsymbol{\beta}$ is allowed to be complex, then (19) remains valid, but $\hat{\boldsymbol{\beta}}(\omega)$ has a complex multivariate normal distribution. Inference about the optimal (complex) scaling vector can be performed following Brillinger (1975, thms. 9.4.3 and 9.4.4), wherein the asymptotic $(n, m \to \infty)$ covariance matrix of the sample optimal scaling $\hat{\boldsymbol{\beta}}(\omega)$, say $\boldsymbol{\Sigma}_{\boldsymbol{\beta}}(\omega)$, is given by

$$\boldsymbol{\Sigma}_{\boldsymbol{\beta}}(\omega) = \nu_m^{-2}\lambda_1(\omega)\sum_{l=2}^{p}\lambda_l(\omega)\{\lambda_1(\omega)-\lambda_l(\omega)\}^{-2}\boldsymbol{\beta}_l(\omega)\boldsymbol{\beta}_l^*(\omega),$$

where $\{\lambda_1(\omega) = \lambda(\omega), \lambda_2(\omega), \ldots, \lambda_p(\omega)\}$ are the latent roots of $\mathbf{V}^{-1}\mathbf{f}_{\mathbf{Y}}(\omega)$ arranged in decreasing order and $\{\boldsymbol{\beta}_1(\omega) = \boldsymbol{\beta}(\omega), \boldsymbol{\beta}_2(\omega), \ldots, \boldsymbol{\beta}_p(\omega)\}$ are the corresponding latent vectors. This result may be used to form an asymptotic test for $\boldsymbol{\beta}(\omega)$ by approximating the distribution of

$$2(\hat{\boldsymbol{\beta}}(\omega) - \boldsymbol{\beta}(\omega))^*\hat{\boldsymbol{\Sigma}}_{\boldsymbol{\beta}}^{+}(\omega)(\hat{\boldsymbol{\beta}}(\omega) - \boldsymbol{\beta}(\omega)) \tag{23}$$

by a chi-squared distribution with $2(p-1)$ degrees of freedom. In (23), $\hat{\boldsymbol{\Sigma}}_{\boldsymbol{\beta}}(\omega)$ is the estimate of $\boldsymbol{\Sigma}_{\boldsymbol{\beta}}(\omega)$ and $^+$ denotes a Moore–Penrose inverse. One can use (23) to check whether or not a particular element is 0, as discussed for the real case, by inserting $\hat{\boldsymbol{\beta}}(\omega)$ into (23), but with the particular element zeroed out and the resulting vector rescaled to be of

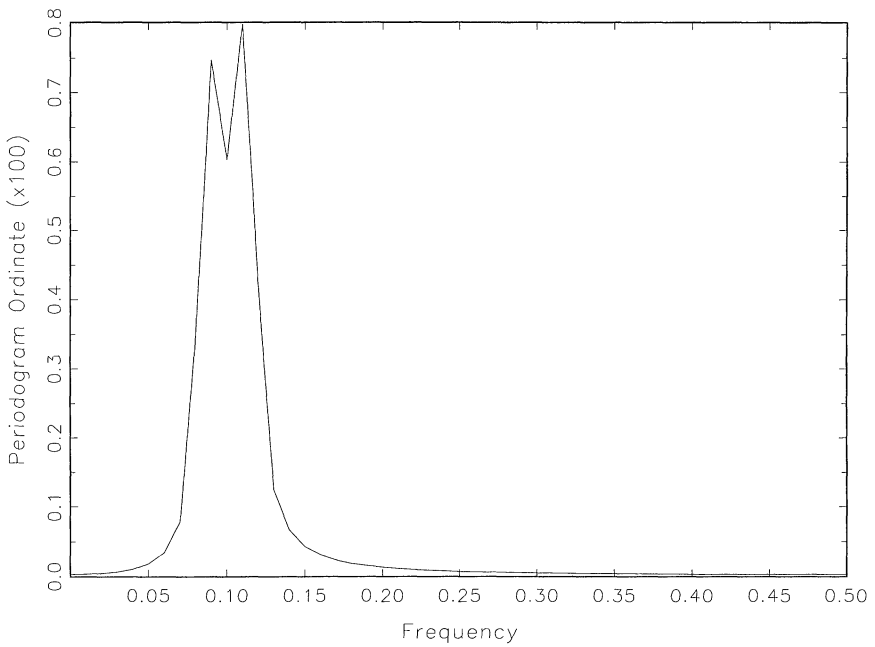

Figure 6. Periodogram of the Expected Signal Shown in Figure 5.

unit length. Alternately, one may use this result to form confidence regions for the components, $\hat{\beta}_{1,j}(\omega), j = 1, \ldots, p$, of the optimal scaling vector by approximating the distribution of

$$\frac{2|\hat{\beta}_{1,j}(\omega) - \beta_{1,j}(\omega)|^2}{s_j^2(\omega)} \tag{24}$$

by a chi-squared distribution with 2 degrees of freedom. In (24), $s_j^2(\omega)$ is the jth diagonal element of $\hat{\boldsymbol{\Sigma}}_{\beta}(\omega)$. One can use (24) to check whether or not the value of 0 is in the confidence region by comparing $2|\hat{\beta}_{1,j}(\omega)|^2/s_j^2(\omega)$ with $\chi_2^2(1-\alpha)$, the $1-\alpha$ upper tail cutoff of the χ_2^2 distribution.

Caution should be used when applying (21), (23), or (24) due to the fact that for the asymptotics to be valid, the smoothing value, m, must be large. In some situations, making m too large can smooth away peaks in the spectral envelope, especially when the signals are extremely narrow band signals. Consequently, one might consider repeating the analysis for various values of m.

Example 2. To test these methods, I generated 12 time series of length $n = 128$ under various conditions. In each case, the $\varepsilon_j(t)$, are iid N(0, 1), for $j = 1, \ldots, 12$, and $t = 1, \ldots, 128$. The first four series are of the form

$$Y_j(t) = c_j \cos(2\pi t\omega_a) + \varepsilon_j(t) + .5\varepsilon_j(t-1), \qquad j = 1, \ldots, 4,$$

where $\omega_a = .1$ (which is not a Fourier frequency) and the amplitudes (which were chosen on an arbitrary basis to be smaller than the standard deviation of the noise term) are $c_1 = .59, c_2 = .36, c_3 = .87$, and $c_4 = .21$. Note that these four series are in phase; also, I have departed from the basic model assumption and added colored noise in the form of a moving average. The next four series were generated as

$$Y_j(t) = c_j \cos(2\pi[t\omega_b + \tau_j]) + \varepsilon_j(t) - .5\varepsilon_j(t-1), \qquad j = 5, \ldots, 8,$$

where $\omega_b = 32/128 = .25, \tau_j$ are iid U(0, 1), and the amplitudes are $c_5 = .62, c_6 = .39, c_7 = 1.06$, and $c_8 = .54$. Note that these four series are not in phase. The next two series are a mixture of the two types:

$$Y_j(t) = c_{1j} \cos(2\pi t\omega_a) + c_{2j} \cos(2\pi[t\omega_b + \tau_j]) + \varepsilon_j(t) + .5\varepsilon_j(t-1), \qquad j = 9, 10,$$

where $c_{1,9} = .34, c_{2,9} = .37, c_{1,10} = .84$, and $c_{2,10} = .48$. Finally, the last two series have no signals:

$$Y_j(t) = \varepsilon_j(t) - .5\varepsilon_j(t-1), \qquad j = 11, 12.$$

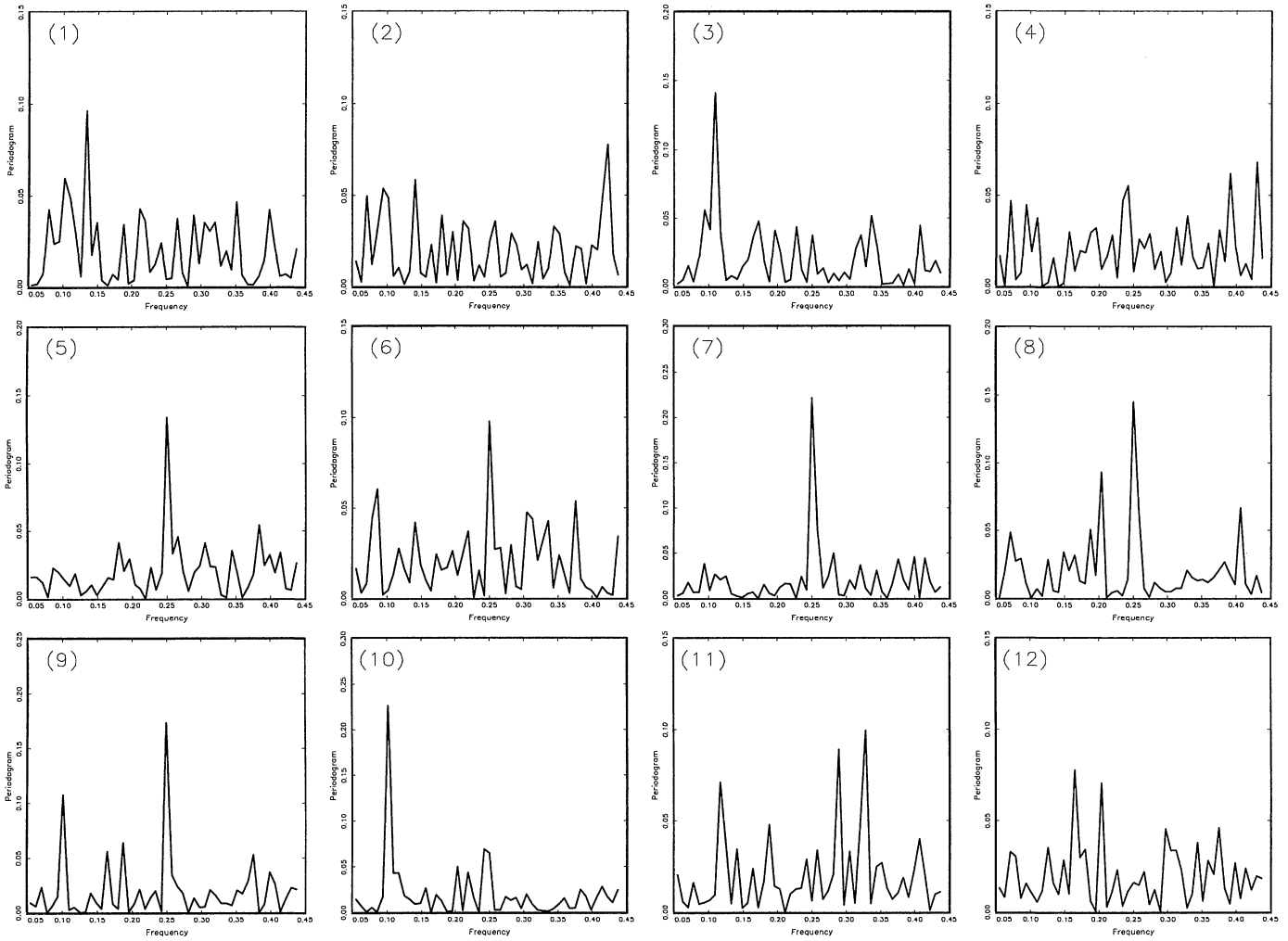

Figure 7. Periodograms of the Time Series $Y_j(t)$, for $j = 1, \ldots, 12$, Generated in Example 4.

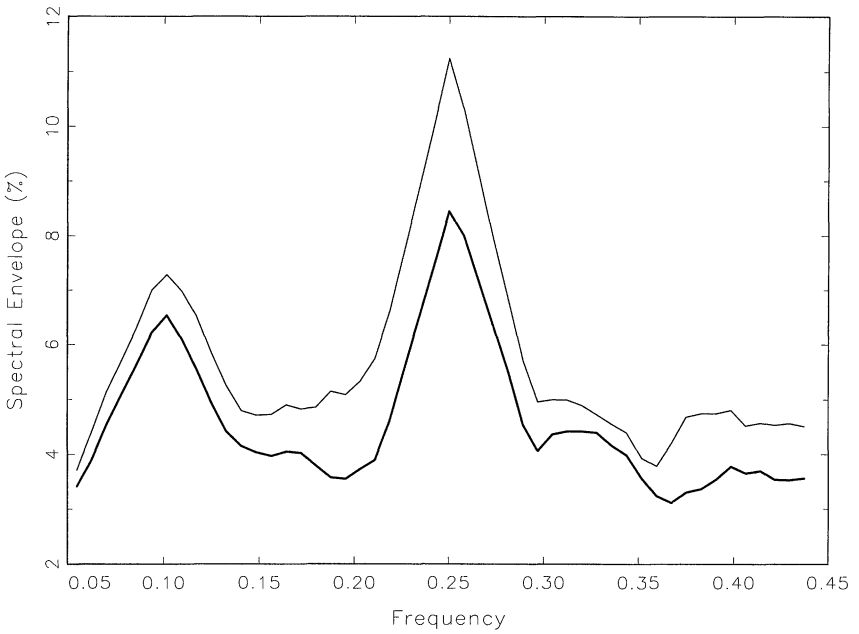

Figure 8. Spectral Envelopes of the 12 Time Series Generated in Example 4, Based on Complex Scales (Thin Line) and on Real Scales (Thick Line).

The periodograms of the generated series are shown in Figure 3. The general appearance of the periodograms in Figure 3 is somewhat contrary to what is known to be true. For example, it is known that series 1–4, 9, and 10 contain a signal at frequency .10, but it appears from the periodograms that series 2 and 4 do not. In addition, it is known that the series 5–8, 9, and 10 contain a signal at frequency .25, but it appears that 6 and 10 do not.

Figure 4 shows the spectral envelopes using complex scales (thin line) and real scales (thick line). Both techniques clearly identify the frequencies of .10 and .25. In both cases, the spectral envelope was estimated using triangular smoothing with $m = 7$ and weights $\{h_0 = 7/49, h_1 = 6/49, h_2 = 5/49, \ldots, h_7 = 1/49\}$. Note that because the real-valued case is a special case of the complex-valued approach, the "real" spectral envelope is never above the "complex" spectral envelope.

Table 3. Example 4 Results for Frequency ω = .10

Series	Amplitude	δ	Complex scale[a,b]	Real scale[a,c]
1	.59	−.001	.47 (123.99)	.39 (25.06)
2	.36	.002	.38 (352.81)	.40 (58.62)
3	.87	.003	.48 (322.42)	.47 (56.76)
4	.21	.003	.27 (59.13)	.21 (12.91)
5	0		.18 (22.14)	.15 (6.26)
6	0		.02 (.43)	.04 (.50)
7	0		.09 (3.88)	.06 (.63)
8	0		.01 (.06)	.01 (.05)
9	.34	0	.34 (275.14)	.38 (40.30)
10	.84	.003	.40 (55.01)	.48 (30.82)
11	0		.06 (1.86)	.04 (.34)
12	0		.12 (5.20)	.14 (5.50)

NOTE: [a]Values shown are the absolute values of the particular scale.
[b]The value of the test statistic based on (23) is shown in parentheses; compare cautiously to a χ^2_{22}.
[c]The value of the test statistic based on (21) is shown in parentheses; compare cautiously to a χ^2_{10}.

Tables 1 and 2 show the complex and real scales at the selected frequencies of 0.10 and 0.25. Except for one case, Table 2, series 2, using the complex version, the conclusions reached from this analysis are the correct conclusions using both the complex version and the real version of the spectral envelope.

3. RANDOM FREQUENCY EFFECTS

In this section I focus on the case where some series contain signals that may be only approximately the same. To accomplish this, I model frequency as a random effect. My basic model is still (5), but I make some different assumptions about the K signals. As in the previous section, I assume that each signal is associated with a particular frequency (which are well separated), and, because I am using the spectral envelope, I eventually focus on the single-signal model. I motivate the ideas with an example.

Example 3. Suppose that the time series of interest $Y_j(t)$ follow the model

$$Y_j(t) = \mu_j + c_j S_j(t) + \varepsilon_j(t), \qquad j = 1, \ldots, p, \quad (25)$$

where μ_j is the level of the jth series and $\varepsilon_j(t)$ are independent white noise processes with variance σ_j^2 that are independent of the signals. The amplitude of the jth signal is c_j (which may be 0), where the random signals are given by

$$S_j(t) = \cos(2\pi[\omega_0 + \delta_j]t + 2\pi\tau_j). \quad (26)$$

In (26), τ_j is a fixed phase, ω_0 is the common frequency, and δ_j for $j = 1, \ldots, p$ are independent random uniform perturbations, with $\delta_j \sim U(-\Delta, \Delta)$ and $\Delta \geq 0$ is some small amount.

In this model the frequency corresponding to each time series is a random effect, so the series are allowed to be

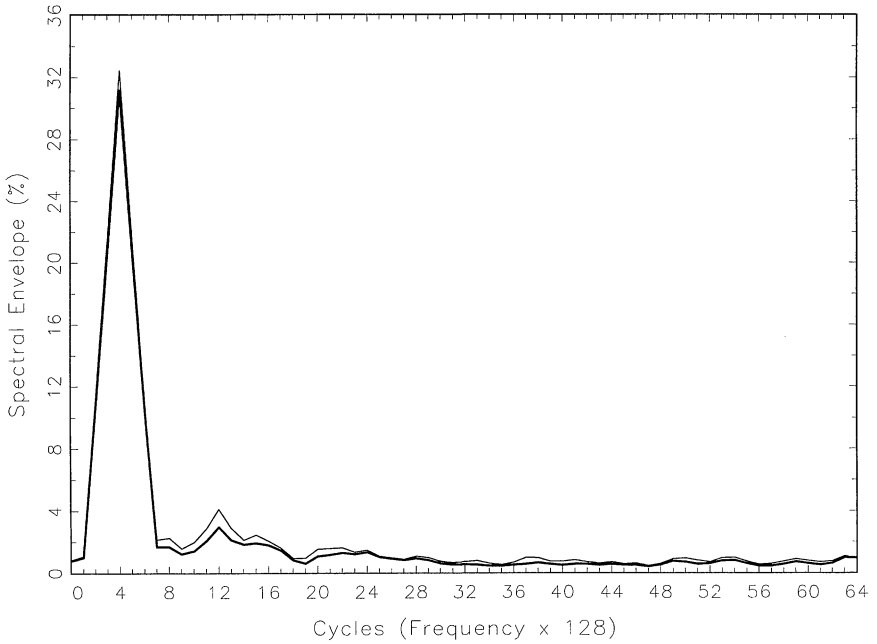

Figure 9. The Sample Spectral Envelopes, $\hat{\lambda}(\omega)$ (Complex Version, Thin Line; Real Version, Thick Line), for the Awake-Shock Stimulus Condition. The peak in the spectral envelope occurs at the frequency ω = 4/128.

only approximately the same. In addition, ω_0 need not be a Fourier frequency. The expected behavior of the signal is

$$E\{S_j(t)\} = \frac{1}{2\Delta}\int_{-\Delta}^{\Delta} \cos\{2\pi(\omega_0+\delta)t + 2\pi\tau_j\}\, d\,\delta$$
$$= \cos(2\pi[\omega_0 t + \tau_j])\ \text{sinc}\ (2\pi\Delta t), \qquad (27)$$

using the definition $\text{sinc}(u) \equiv \sin(u)/u, u \neq 0$, and $\text{sinc}(0) \equiv 1$. As a general statement, (27) implies that the particular signals given in (26) satisfy the general property that

$$E\{S_j(t)\} = S_0(t-\tau_j)\kappa(\Delta t), \qquad (28)$$

where $S_0(t-\tau_j)$ is a fixed harmonic signal (with arbitrary phase) that oscillates at frequency ω_0 and $\kappa(\Delta t)$ is a taper controlled by Δ; the larger the value of Δ, the more dramatic the taper, and when $\Delta = 0$, the taper has no effect.

Figure 5 shows an example of (27) with $n = 100, \omega_0 = .1$, and $\Delta = .1/(2\pi) = .016$. This means that the time series analyzed can have periods of oscillation ranging between about 8.5 cycles (1/.116) and about 12 cycles (1/.084) in 100 observations. Hence this value of Δ would be considered rather large. However, a Fourier analysis is still a viable solution, as is seen from the periodogram of (27) shown in Figure 6. Note that the periodogram is spread out around ω_0, and hence smoothing the periodogram would be wise in this type of situation. This is because the expected signal is of the form $\cos(\omega_0 t)\sin(\Delta t)$, where Δ is small. But

$$2\cos(\omega_0 t)\sin(\Delta t) = \sin([\omega_0+\Delta]t) - \sin([\omega_0-\Delta]t),$$

and hence the twin peaks seen in Figure 6.

Now considering the DFTs of the data, (6), as in (7), the model (25) can be written as

$$d_{Y_j}(\omega) = a_j d_{S_j}(\omega) + d_{\varepsilon_j}(\omega) \qquad j = 1,\ldots,p, \qquad (29)$$

where $a_j = c_j \exp(-2\pi i \tau_j \omega)$, $d_{S_j}(\omega)$ is the DFT of the individual random signal term $\cos(2\pi[\omega_0+\delta_j]t)$, and $d_{\varepsilon_j}(\omega)$ is the DFT of the individual noise terms. To investigate (29), it is easier to work with the complex version of the signal; that is, let

$$S_j(t) = \exp\{2\pi i(\omega_0+\delta_j)t\}.$$

Then, as in (27),

$$E\{d_{S_j}(\omega)\} = n^{-1/2}$$
$$\times \sum_{t=1}^{n} \exp\{-2\pi i(\omega-\omega_0)t\}\ \text{sinc}(2\pi\Delta t), \qquad (30)$$

which is the tapered (by the sinc kernel) transform of $\exp(2\pi i\omega_0 t)$. In addition, as seen in Figure 6, the modulus of $E\{d_{S_j}(\omega)\}$ will be extremely close to the modulus of the finite transform of $\exp(i\omega_0 t)$, provided that Δ is not too large relative to n.

The individual series, $Y_j(t)$, are coherent with each other, provided that their respective signal amplitudes are not 0. If in (29) $a_j a_k = 0$ for any pair $j,k = 1,\ldots,p$, then

$$E\{d_{Y_j}(\omega)d^*_{Y_k}(\omega)\} = \sigma_j^2 I_{\{0\}}(j-k), \qquad (31)$$

where σ_j^2 is the variance of $\varepsilon_j(t)$ and $I_A(\cdot)$ is the indicator of the set A. If $|a_j a_k| > 0$ when $j \neq k$, then

$$E\{d_{Y_j}(\omega)d^*_{Y_k}(\omega)\} = a_j a_k E\{d_{S_j}(\omega)\}E\{d^*_{S_k}(\omega)\}, \qquad (32)$$

where $E\{d_{S_j}(\omega)\}$ was given in (30). If $|a_j| > 0$, then

$$E\{|d_{Y_j}(\omega)|^2\} = |a_j|^2 E\{|d_{S_j}(\omega)|^2\} + \sigma_j^2, \qquad (33)$$

where

$$E\{|d_{S_j}(\omega)|^2\} = \sum_{|h|<n}\left(1-\frac{|h|}{n}\right)$$
$$\times \exp\{-2\pi i(\omega-\omega_0)h\}\ \text{sinc}(2\pi\Delta h).$$

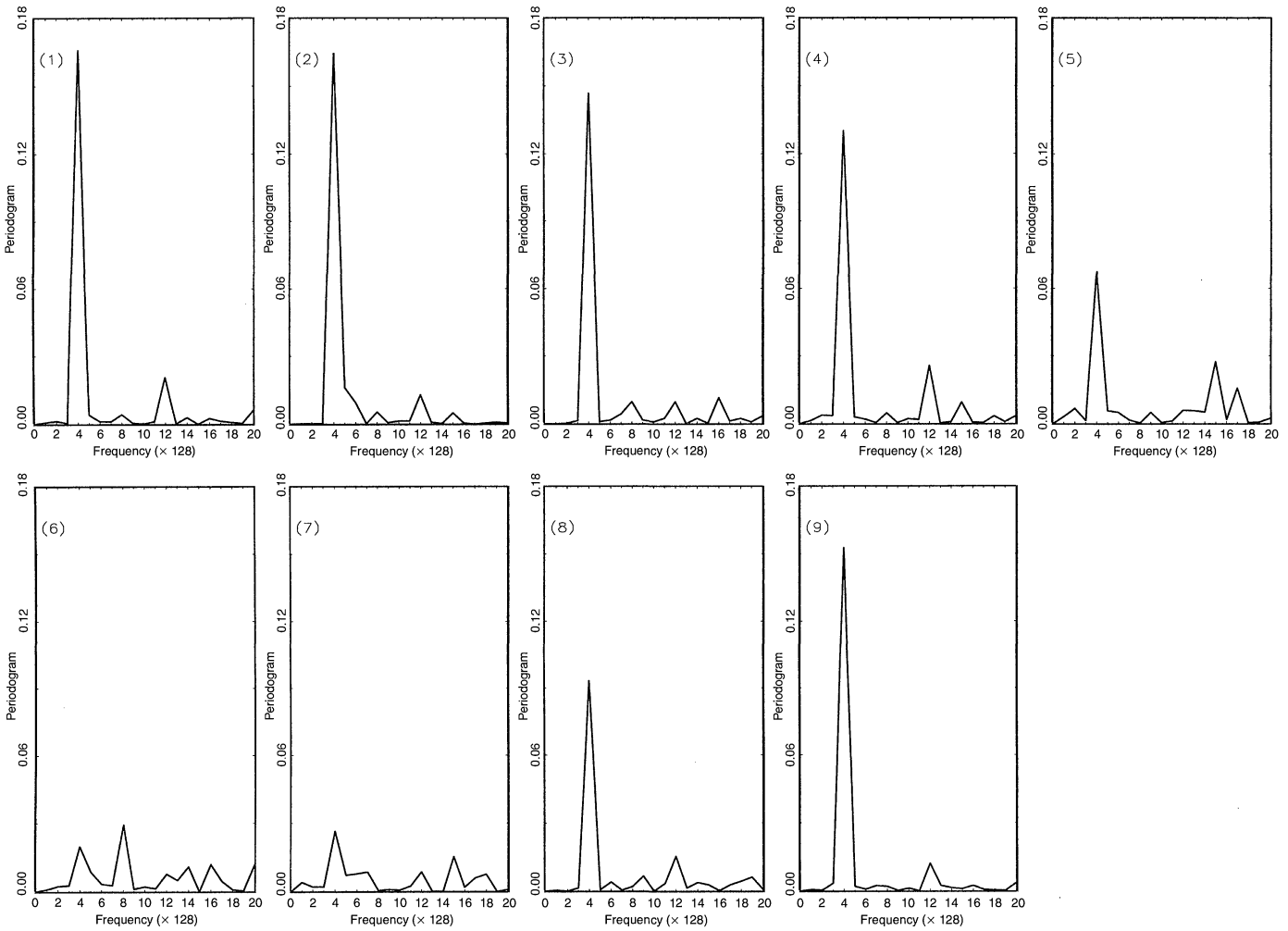

Figure 10. Periodograms of the Awake-Shock Series $Y_j(t)$, for $j = 1, \ldots, 9$, Representing Locations [L1]–[L9].

A key point made in Example 3 is that even in the situation of (25)–(26), one may carry out an analysis similar to that outlined in the previous section. That is, rather than focus on the p individual transforms, one can use the interrelationships inherent in the model to help identify ω_0. To do this, one makes use of the cross-spectra among the p time series $Y_j(t)$ for $j = 1, \ldots, p$. This enhances the analysis, because if a particular series contains the harmonic component of interest but with a low amplitude or a lot of noise, then an individual analysis may miss this fact, but this particular series may match well with other series containing the harmonic. This particular effect was seen in Example 2.

As a general model (for the case where $K = 1$), take the form of (25) in Example 3; that is,

$$Y_j(t) = \mu_j + c_j S_j(t) + \varepsilon_j(t), \qquad j = 1, \ldots, p. \quad (34)$$

But where the signals $S_j(t)$ belong to the general class of modulated harmonic signals given by

$$S_j(t) = g(t)\cos(2\pi[\omega_0 + \delta_j]t + 2\pi\tau_j), \quad (35)$$

where $g(t)$ does not annihilate the basic common signal, $S_0(t) = \cos(2\pi\omega_0 t)$. In (35) ω_0 is a fixed frequency and δ_j, for $j = 1, \ldots, p$, are independent $U(-\Delta, \Delta)$ random variables, where $\Delta \geq 0$ is some small value and τ_j is a fixed, but unknown phase. An example of a typical modulator is the function $g(t) = \alpha t \exp(-\gamma t)$, where α and $\gamma > 0$ are constants; in this case the signal dampens over time. Another standard example of a modulator is $g(t) = \sin(2\pi\Delta t)$. Note that the $S_j(t)$ in (35) satisfy the general relationship of (28); that is,

$$E\{S_j(t)\} = S_0(t - \tau_j)\kappa(\Delta t), \quad (36)$$

where $S_0(t)$ is a fixed harmonic signal that oscillates at frequency ω_0 and $\kappa(\Delta t)$ is a taper that does not annihilate $S_0(t)$. In fact, one could use (36) as a general definition of the signals, $S_j(t)$, in (34). Of course, (34) may be extended to the case where $K > 1$, as in (5), in an obvious way.

As in Example 3, (29), the model can be written in terms of the DFTs,

$$d_{Y_j}(\omega) = a_j d_{S_j}(\omega) + d_{\varepsilon_j}(\omega), \qquad j = 1, \ldots, p, \quad (37)$$

where $a_j = c_j \exp(-2\pi i \tau_j \omega)$, $d_{S_j}(\omega)$ is the DFT of the individual random signal term satisfying (35), and $d_{\varepsilon_j}(\omega)$ is the DFT of the individual noise terms. In particular, $E\{d_{S_j}(\omega)\}$ is the DFT of $S_0(t)\kappa(\Delta t)$, where now the taper is of the form $\kappa(\Delta t) = g(t)\mathrm{sinc}(2\pi\Delta t)$.

Let $\mathbf{Y}(t) = (Y_1(t), \ldots, Y_p(t))'$ and let $\mathbf{d}_\mathbf{Y}(\omega)$ denote the $p \times 1$ vector of finite transforms with jth component $d_{Y_j}(\omega)$. As in Section 2, arrange the vector so that for $0 \le q \le p, a_{q+1} = \cdots = a_p = 0$, and none of the $\{a_1, \ldots, a_q\}$ are 0. Then (37) can be written as

$$\mathbf{d}_\mathbf{Y}(\omega) = \mathbf{A}\mathbf{d}_S(\omega) + \mathbf{d}_\varepsilon(\omega), \tag{38}$$

where $\mathbf{A}$ is the $p \times p$ complex diagonal matrix $\mathbf{A} = \operatorname{diag}\{a_1, \ldots, a_q, 0, \ldots, 0\}$ and $\mathbf{d}_S(\omega)$ and $\mathbf{d}_\varepsilon(\omega)$ are the $p \times 1$ vectors of transforms with jth component $d_{S_j}(\omega)$ and $d_{\varepsilon_j}(\omega)$.

Let $\mathbf{f}_\mathbf{Y}(\omega) = E\{\mathbf{d}_\mathbf{Y}(\omega)\mathbf{d}_\mathbf{Y}^*(\omega)\}$ be the $p \times p$ complex matrix with elements given by the values in (31)–(33), with $\operatorname{sinc}(2\pi\Delta t)$ replaced by the general form $\kappa(\Delta t)$. In an obvious way, based on (38), decompose the elements of $\mathbf{f}_\mathbf{Y}(\omega)$ as

$$\mathbf{f}_\mathbf{Y}(\omega) = \mathbf{A}\mathbf{f}_S(\omega)\mathbf{A}^* + \mathbf{f}_\varepsilon(\omega), \tag{39}$$

where $\mathbf{A}\mathbf{f}_S(\omega)\mathbf{A}^*$ is a Hermitian block-diagonal matrix and $\mathbf{f}_\varepsilon(\omega) = \operatorname{diag}\{\sigma_1^2, \ldots, \sigma_p^2\}$. This situation is somewhat different than that discussed in Section 2, however. Here (39) is a type of complex factor analytic representation for $\mathbf{f}_\mathbf{Y}(\omega)$; that is, $\mathbf{f}_\mathbf{Y}(\omega)$ is the sum of a rank $r \le q \le p$ nonnegative-definite matrix $\mathbf{A}\mathbf{f}_S(\omega)\mathbf{A}^*$ and a positive-definite diagonal matrix $\mathbf{f}_\varepsilon(\omega)$. If $\Delta = 0$, then this model is the model of Section 2, in which case $r = 1$. The elements of the matrix $\mathbf{f}_S(\omega)$ depend on n, κ, Δ, and ω_0. In particular, using (30), (32), and (33), the off-diagonal elements of $\mathbf{f}_S(\omega)$ are of the form (to ease the discussion I use the complex version of the signal)

$$f_{S_{jk}}(\omega) = n^{-1}\left|\sum_{t=1}^{n} \exp\{-2\pi i(\omega - \omega_0)t\}\kappa(\Delta t)\right|^2, \qquad j \ne k = 1, \ldots, p, \tag{40}$$

and the diagonal elements are

$$f_{S_{jj}}(\omega) = \sum_{|h|<n}\left(1 - \frac{|h|}{n}\right) \times \exp\{-2\pi i(\omega - \omega_0)h\}\kappa(\Delta h), \qquad j = 1, \ldots, p. \tag{41}$$

For ω far from ω_0, $f_S(\omega)$ is approximately the zero matrix (recall that I do not assume that ω_0 is a Fourier frequency), because its elements are convoluted Dirichlet kernels evaluated away from 0. As previously mentioned, the situation in Section 2 can be thought of as the case where $\Delta = 0$ and $g(t)$ is constant, in which case all of the elements of $\mathbf{f}_S(\omega)$ are the same, implying that the rank, r, of $\mathbf{f}_S(\omega)$ is 1.

My preference is to work with the standardized series $\mathbf{Z}(t) = \mathbf{V}^{-1/2}\mathbf{Y}(t)$, where $\mathbf{V}$ is the diagonal matrix of variances defined in Section 2. Thus with $\mathbf{f}_\mathbf{Z}(\omega) = \mathbf{V}^{-1/2}\mathbf{f}_\mathbf{Y}(\omega)\mathbf{V}^{-1/2}$ as in (12), put

$$\mathbf{B}(\omega)\mathbf{B}^*(\omega) = \mathbf{V}^{-1/2}\mathbf{A}\mathbf{f}_S(\omega)\mathbf{A}^*\mathbf{V}^{-1/2} \tag{42}$$

and

$$\begin{aligned}\mathbf{D}(\omega) &= \mathbf{V}^{-1/2}\mathbf{f}_\varepsilon(\omega)\mathbf{V}^{-1/2} \\ &= \operatorname{diag}\{\sigma_1^2/\sigma_{Y_1}^2, \ldots, \sigma_p^2/\sigma_{Y_p}^2\},\end{aligned} \tag{43}$$

and write the model as

$$\mathbf{f}_\mathbf{Z}(\omega) = \mathbf{B}(\omega)\mathbf{B}^*(\omega) + \mathbf{D}(\omega), \tag{44}$$

noting that $\mathbf{B}(\omega)$ is a $p \times q$ matrix such that all of the elements in the final $p - q$ rows of $\mathbf{B}(\omega)$ are 0, and $\operatorname{rank}(\mathbf{B}(\omega)) = r \le q$.

Note that it is not necessary to assume that the $S_j(t)$ are sinusoidal as in (35). In fact, the basic results are the same if one is willing to assume only that the $S_j(t)$ satisfy the relationship described in (36). Estimation of the spectral envelope and optimal scalings is accomplished by smoothing

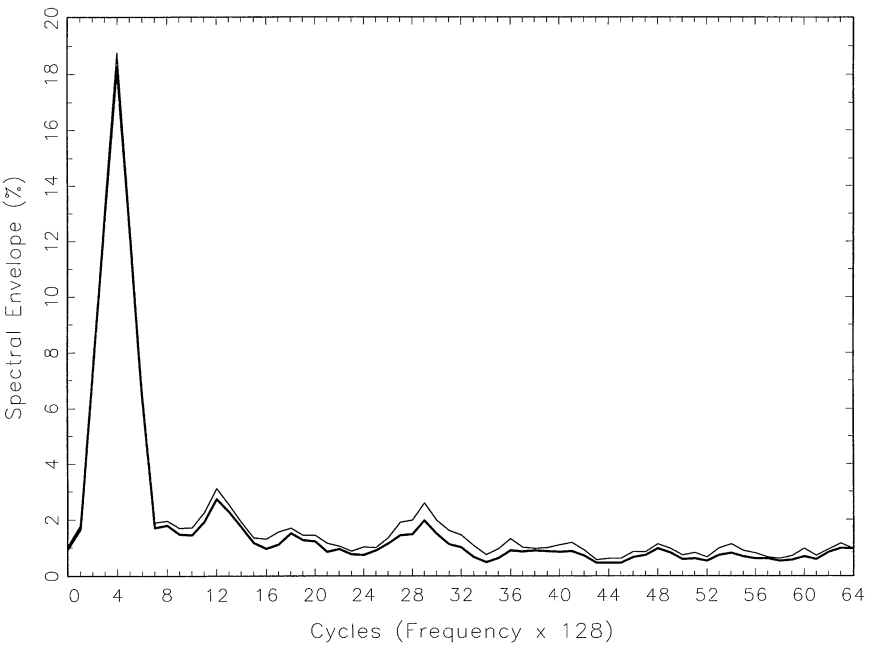

Figure 11. The Sample Spectral Envelope, $\hat{\lambda}(\omega)$ (Complex Version, Thin Line; Real Version, Thick Line), for the High-Brush Stimulus Condition. The peak in the spectral envelope occurs at the frequency ω = 4/128.

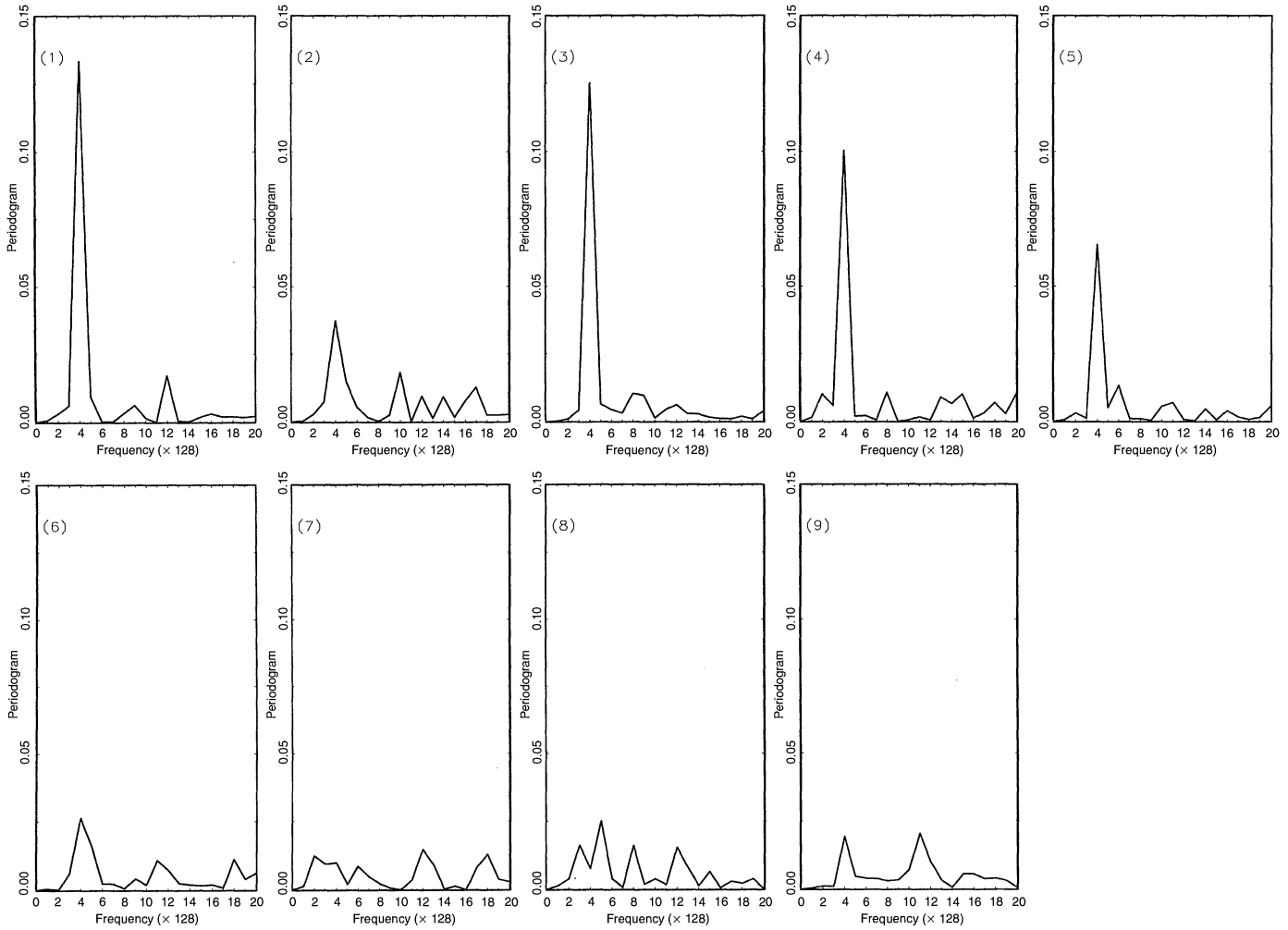

Figure 12. Periodograms of the High-Brush Series $Y_j(t)$, for j = 1, ... , 9, Representing Locations [L1]–[L9].

the periodograms as in (17) and (18) so that cross-spectra can be estimated. This is reasonable even near ω_0, because one expects the spectra to be spread out around this frequency, as seen in (40) and (41).

Example 4. This example is an extension of Example 2. I again generated 12 series of length $n = 128$ with the same amplitudes and common frequencies as in Example 2, but in this example the noise terms are white. The first four series were generated as

$$Y_j(t) = c_j g(t)\cos(2\pi[\omega_a + \delta_j]t) + \varepsilon_j(t), \qquad j = 1, \ldots, 4,$$

where $\omega_a = .1$ (which is not a Fourier frequency) and $g(t)$ is an exponential modulator given by

$$g(t) = .5t\exp(-t/10).$$

The δ_j are independent $U(-\Delta, \Delta)$, where $\Delta = 1/2(128) = .004$; recall that the amplitudes are $c_1 = .59, c_2 = .36, c_3 = .87$, and $c_4 = .21$. The next four series were generated as

$$Y_j(t) = c_j\cos(2\pi[\omega_b + \delta_j]t + 2\pi\tau_j]) + \varepsilon_j(t), \qquad j = 5, \ldots, 8,$$

where $\omega_b = 32/128 = .25$. The δ_j are also independent $U(-\Delta, \Delta)$, and the amplitudes are as in Example 2; that is, $c_5 = .62, c_6 = .39, c_7 = 1.06$, and $c_8 = .54$. Series $Y_9(t)$ and $Y_{10}(t)$ are generated as the sum of two processes like the first and second sets (with the same amplitudes as in Example 2), but the first component is not modulated:

$$Y_j(t) = c_{1j}\cos(2\pi[\omega_a + \delta_j]t) + c_{2j}\cos(2\pi[\omega_b + \delta_j]t + 2\pi\tau_j]) + \varepsilon_j(t), \qquad j = 9, 10,$$

where $c_{1,9} = .34, c_{2,9} = .37, c_{1,10} = .84, c_{2,10} = .48$, and $\delta_j \sim U(-\Delta, \Delta)$. The last two series, $Y_{11}(t)$ and $Y_{12}(t)$, are Gaussian white noise.

Figure 7 shows the individual periodograms, which are similar to those of Example 2 (see Fig. 3). Figure 8 shows the spectral envelope of the data. Note that the power in the envelope at frequency .10 is much smaller here than in Figure 4, but the envelope still identifies both the .10 and .25 frequencies as important. Table 3 gives the results of the frequency .10 analysis; the results for the .25 frequency are similar. As in Example 2, although an individual periodogram analysis would lead to the wrong conclusions (e.g., periodograms 1, 2, and 4 in Fig. 7 show no evidence of the .10 harmonic), the spectral envelope leads to the appropriate conclusions.

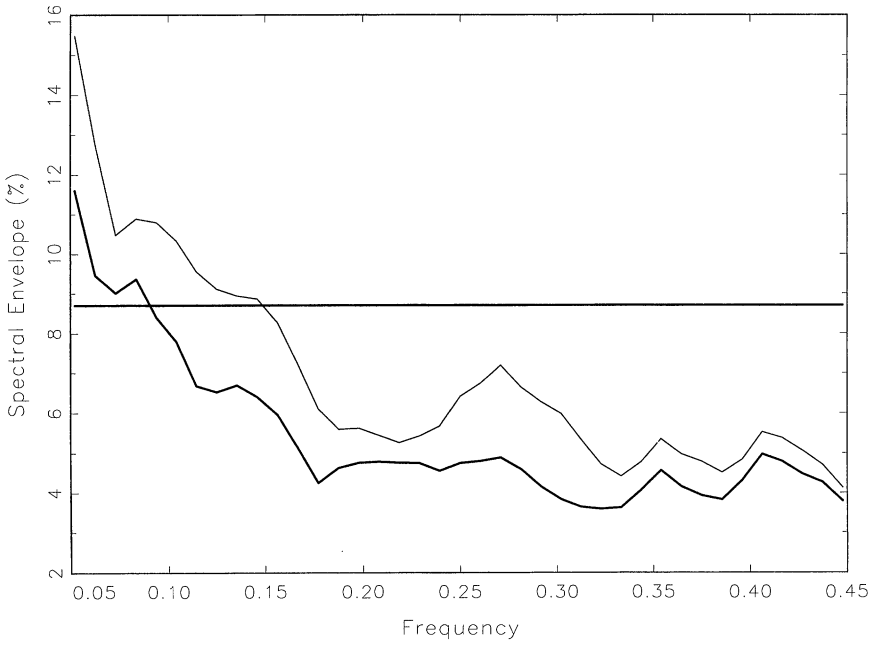

Figure 13. Sample Spectral Envelopes, $\hat{\lambda}(\omega)$, for the Black Group in the Ambulatory Blood Pressure Study Using Complex Scaling (Thin Line) and Real Scaling (Thick Line). The straight line is an approximate $\alpha = 10^{-5}$ significance threshold using (22).

4. APPLICATIONS

Two applications are presented in this section. The first application, already discussed in Example 1, is a case of evoked responses where the experiment is designed and thus corresponds more closely to the discussion in Section 2. The second application is not a designed experiment and would correspond more closely to Section 3 ideas.

4.1 An Experiment in Pain (Example 1 Continued)

This analysis focuses on the study described in Example 1 that used fMRI to examine pain perception in humans. The substantive issues have been reported by Antognini, Buonocore, Disbrow, and Carstens (1998), and I use part of the dataset as an example of the methodology. In particular, I use this example to explore the similarities and differences between the real and complex cases and to investigate how they might also be used to examine phase.

Figure 9 shows the estimated spectral envelope for the stimulus condition awake-shock (the data are shown in Fig. 1) using triangular smoothing with $m = 2$; note that real and complex cases are nearly identical. From this, it can be concluded that the BOLD signals are in phase. There is a clear peak in the sample spectral envelope, $\hat{\lambda}(4/128) = 32.4\%$ (both cases), corresponding to frequency of $\omega = 4$ cycles/128 points or 4/256 Hz, which corresponds to the stimulation period of 64 seconds. The magnitudes of the optimal sample scalings (the complex and real scales are nearly the same) and the corresponding χ^2_2 test given by (2.20) are [L1] .41 (233.4), [L2] .42 (138.4), [L3] .39 (389.5), [L4] .37 (352.7), [L5] .27 (107.2), [L6] .14 (14.0), [L7] .16 (18.8), [L8] .31 (252.8), and [L9] .40 (539.5), indicating that all locations are receiving the shock signal.

Figure 10 shows the individual periodograms at the nine locations [L1]–[L9] for the awake-shock stimulus condition. Note that at locations [L6] and [L7] the signals are very weak, and it is doubtful that an individual analysis would pick up this very weak (but present) signal at these locations.

Next, I repeat the analysis for the high-brush stimulus condition (the data are shown in Fig. 2). Figure 11 displays the sample spectral envelopes (real and complex), which again are nearly identical. In this case the sample spectral envelopes are about 18.8% at the stimulation period, which is a little more than half of the power seen in the case of the awake-shock stimulus condition. This indicates that the high-brush signal is not as strong as the awake-shock signal. The magnitudes of the optimal sample scalings (the complex and real scales are nearly the same) and the corresponding χ^2_2 test given in (24) are [L1] .51 (689.8), [L2] .28 (34.2), [L3] .48 (402.4), [L4] .43 (127.8), [L5] .34 (39.0), [L6] .24 (25.3), [L7] .16 (9.7), [L8] .14 (2.8), and [L9] .18 (17.2), indicating that all locations except for [L8] are receiving the shock signal. Figure 12 displays the individual periodograms; again it appears that a separate analysis of the periodograms would lead to a somewhat different conclusion.

4.2 Ambulatory Blood Pressure and the Bogalusa Heart Study

The Bogalusa Heart Study is a detailed study of children focusing on understanding the early natural history of coronary artery disease and essential hypertension. It is a major program studying a well-defined, biracial (black–white) population of children in a semirural community in Louisiana. The study has conducted cardiovascular risk factor research both in the community and in the laboratory since 1972. Details have been provided by Berenson et al. (1991).

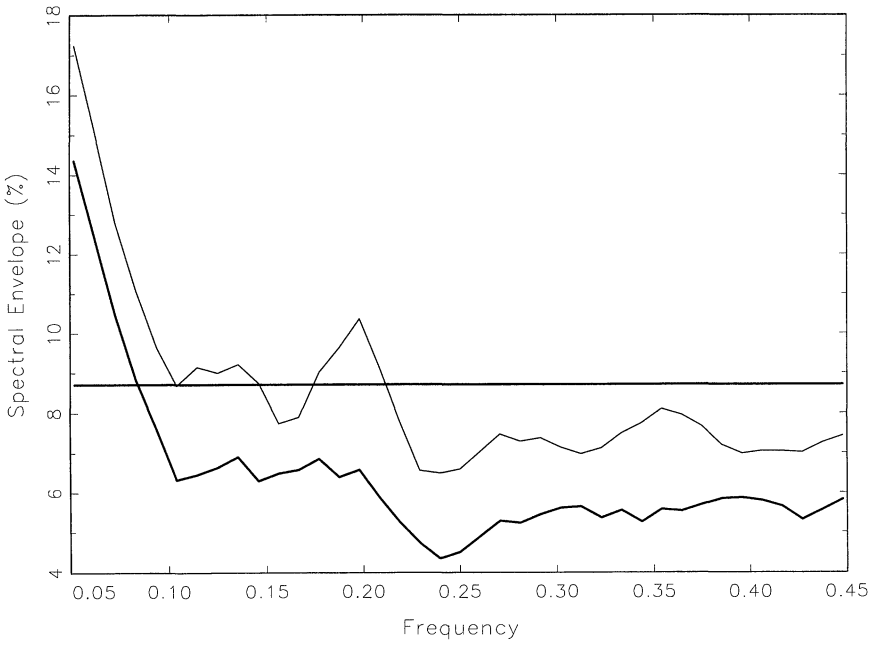

Figure 14. Sample Spectral Envelopes, $\hat{\lambda}(\omega)$, for the White Group in the Ambulatory Blood Pressure Study Using Complex Scaling (Thin Line) and Real Scaling (Thick Line). The straight line is an approximate $\alpha = 10^{-5}$ significance threshold using (22).

Many different substudies have been conducted over the years. These substudies include a special study on ambulatory blood pressure, which is the focus of this analysis. The data collected are ambulatory blood pressure readings taken every 15 minutes for 24 hours on preteens. Subjects wear a noninvasive monitor that measures blood pressure and heart rate at regular intervals throughout the day. The purpose of ambulatory blood pressure monitoring is to obtain data that reflect the cardiovascular state of patients under conditions more representative of their everyday lifestyle than those inherent in a clinical environment.

In this analysis I concentrate on the diastolic blood pressure (DBP) readings of 29 preteens representing fairly evenly blacks (14), whites (15), females (12, of which 6 are black), and males (17, of which 8 are black). A number of techniques are used to screen the data for anomalies (e.g., a DBP reading that exceeds the systolic BP reading). In addition, the data are adjusted for periods of sleep (wherein DBP drops by about 10–20 mm Hg), so that the level of each DBP series is constant.

The raw data were given to me by a cardiologist involved in the heart study a number of years ago. He was interested in finding differences in the cyclic behavior of the blood pressure readings between blacks and whites. It was apparent that the cardiologist had a particular agenda. He had written several controversial articles claiming that by the time they reach age 20, black males have abnormally large hearts due to stress, which increases their risk of cardiovascular disease. How this claim related to these data, or what the cardiologist thought we would find, was not revealed to me. I was intrigued and agreed to perform spectral analyses on the ambulatory blood pressure and heart rate readings without knowing anything about the subjects at the time. Unfortunately, the cardiologist passed away during this period, but I was able to ascertain information about the data from other sources working on the heart study. I never knew what the cardiologist was looking for; the separate analyses lead to nothing interesting, and I found only the expected circadian and ultradian rhythms associated with blood pressure and heart rate. It was this experience that led me to think about random frequency effects and group analyses that do not require the entire group to behave a certain way (as, e.g., in MacNeill 1977).

Figures 13 and 14 show the estimated spectral envelopes for the group of 14 blacks and the group of 15 whites, using triangular weighting with $m = 5$. In addition, each plot shows the approximate $\alpha = 10^{-5}$ significance threshold using (22). From these figures, note that (a) there is a difference between using real scalings and using complex scalings (there is no reason to believe that the signals would be in phase), (b) both groups show the expected low-frequency circadian rhythm, and (c) using complex scalings, the white group shows additional cyclic behavior near $\omega = .20$ (about 1 cycle every 75 minutes), with 10 of the 15 children having this signal. In summary, these findings serve as an example of the viability of this technique, but I hesitate to make any substantive conclusions without further guidance from cardiologists.

[Received July 1998. Revised February 1999.]

REFERENCES

Antognini, J. F., Buonocore, M. H., Disbrow, E. A., and Carstens, E. (1998), "Isoflurane Anesthesia Blunts Cerebral Responses to Noxious and Innocuous Stimuli: A Functional MRI Study," *Life Sciences*, 61, PL349–PL354.

Berenson, G. S., Srinivasan, S. R., Webber, L. S., Nicklas, T. A., Hunter, S. M., Harsha, D. W., Johnson, C. C., Arbeit, M. L., Dalferes, E. Jr., Wattigney, W., Kikuchi, D., and Lawrence, M. (1991), *Cardiovascular*

Risk in Early Life: The Bogalusa Heart Study, Kalamazoo, MI: The Upjohn Company.

Brillinger, D. R. (1981), *Time Series: Data Analysis and Theory* (2nd ed.), San Francisco: Holden-Day.

——— (1980), "Analysis of Variance Problems Under Time Series Models," in *Handbook of Statistics*, Vol. 1, ed. P. R. Krishnaiah, Amsterdam: North-Holland, pp. 237–278.

Geweke, J. F. (1977), "The Dynamic Factor Analysis of Economic Time Series Models," *Latent Variables in Socio-Economic Models*, eds. D. Aigner and A. Goldberger, Amsterdam: North Holland, pp. 365–383.

Hannan, E. J. (1970), *Multiple Time Series*, New York: Wiley.

MacNeill, I. (1977), "A Test of Whether Several Time Series Share Common Periodicities," *Biometrika*, 64, 495–508.

McDougall, A. J., Stoffer, D. S., and Tyler, D. E. (1997), "Optimal Transformations and the Spectral Envelope for Real-Valued Time Series," *Journal of Statistical Planning and Inference*, 57, 195–214.

Ogawa, S., and Lee, T. M. (1990b), "Magnetic Resonance Imaging of Blood Vessels at High Fields: In Vivo and in Vitro Measurements and Image Simulation," *Magnetic Resonance in Medicine*, 16, 9–18.

Ogawa, S., Lee, T. M., Nayak, A., and Glynn, P. (1990a), "Oxygenation-Sensitive Contrast in Magnetic Resonance Image of Rodent Brain at High Magnetic Fields," *Magnetic Resonance in Medicine*, 14, 68–78.

Stoffer, D. S., Tyler, D. E., and McDougall, A. J. (1993), "Spectral Analysis for Categorical Time Series: Scaling and the Spectral Envelope," *Biometrika*, 80, 611–622.